RERTR 2012 — 34th INTERNATIONAL MEETING ON
REDUCED ENRICHMENT FOR RESEARCH AND TEST REACTORS

October 14-17, 2012
Warsaw Marriott Hotel
Warsaw, Poland

Mechanical Modeling of U-Mo Fuel Swelling in Monolithic Plates

Yeon Soo Kim, G.L. Hofman, J.S. Cheon *
GTRI Convert Program, Nuclear Engineering Division
Argonne National Laboratory
9700 S. Cass Ave., Argonne, IL 60439-4803 – USA

A.B. Robinson, D.M. Wachs
Idaho National Laboratory
P.O. Box 1625, Idaho Falls, ID 83415-6188 – USA

* Assigned to the GTRI-CONVERT Program at ANL from KAERI

ABSTRACT

Tapering of U-Mo alloy fuel at the end of plates is attributed to lateral mass transfer by fission induced creep, by which fuel mass is relocated away from the fuel end region where fission product induced fuel swelling is in fact the highest. Thanks to this mechanism, U-Mo fuel can achieve high burnup, effectively relieving stresses building up at the fuel end region, in which peak stresses are otherwise expected because peak fission product induced fuel swelling occurs there. ABAQUS FEA was employed to examine whether the observed phenomenon can be simulated using physical-mechanical data available in the literature. The simulation results obtained for several samples with different type and loading scheme showed that the measured data were able to be simulated with a reasonable creep rate coefficient. The obtained creep rate constant is 500×10^{-25} cm^3/MPa, which lies between pure uranium and MOX, and is greater than all other ceramic uranium fuels.

1. Introduction

Two forms of U-Mo alloy fuel have been irradiation-tested in the US GTRI (Global Threat Reduction Initiative) in order to qualify this fuel for the conversion of research and test reactors from HEU to LEU - a fuel particle dispersion in an aluminum matrix and a monolithic fuel foil directly bonded to cladding. The former is called a dispersion fuel and the latter a monolithic fuel. The fueled zone with fuel particles dispersed in the Al matrix in the dispersion fuel plate is called a fuel meat. The geometry for both fuel forms is most frequently a thin plate. When such a

 Work supported by the U.S. Department of Energy, National Nuclear Security Administration's (NNSA's) Office of Defense Nuclear Nonproliferation.

plate is loaded in a test capsule or a real fuel element, both ends of the plate in the width direction are inserted in small grooves, called side rails. Fig. 1 schematically illustrates the cross section of a monolithic fuel plate.

U-Mo fuel swelling only increases the plate thickness because the other dimensions are constrained. Consequently, fuel swelling can be fairly accurately estimated by measuring the fuel thickness during post-irradiation analyses. U-Mo fuel swelling kinetics as a function of fission density is previously documented [1]. U-Mo fuel swelling we are dealing with is at typical irradiation temperatures lower than, say, 250^{o}C in research and test reactors, so the temperature effect is usually neglected.

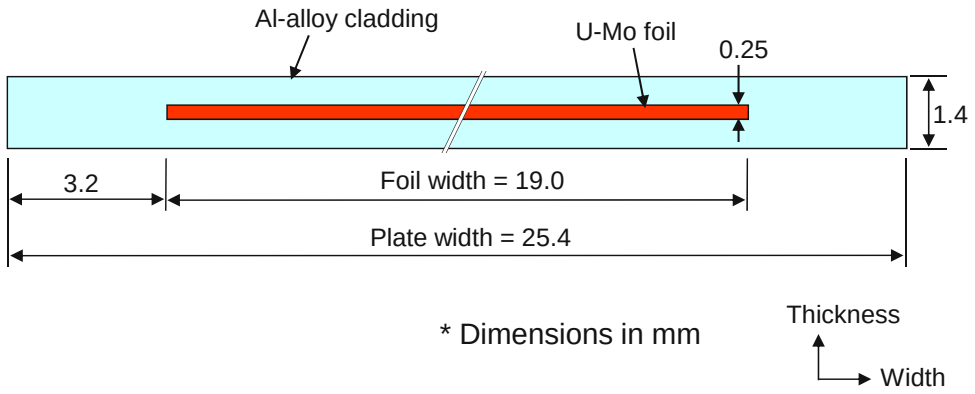

Fig. 1 Schematic of cross section at the axial mid-plane of a monolithic test plate.

In the postirradiation examination (PIE) of fuel plates, it is a common observation that the fuel meat or foil swelling close to the side rails of the plates is significantly diminished, and sometimes negligible. This phenomenon is clearly observable in some RERTR plates where one of the plate width ends faces the ATR core, resulting in a large power peaking at the foil end, and therefore, peaking in fission density occurs there. This is an obvious contradiction according to the fuel swelling kinetics (see Fig. 2).

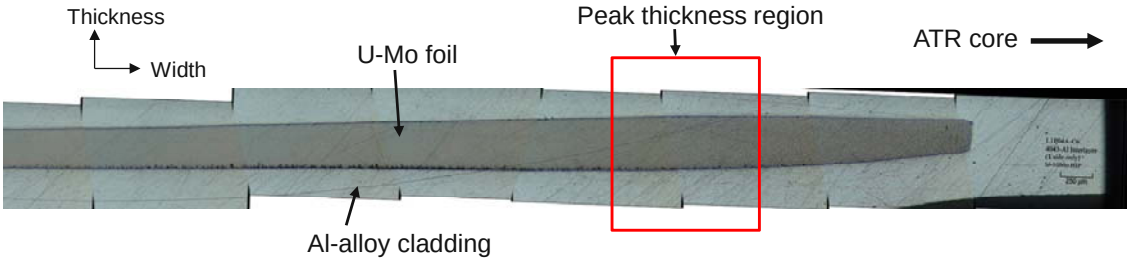

Fig. 2 Fuel plate cross section in the width direction at near the ATR-core side end of L1P04A.

The most plausible causes for this phenomenon are lateral fuel transport toward the fuel center in the width direction and accumulation of fuel mass at regions away from the foil end. The driving force for the fuel volume transport is the shear stress that builds up because of fission product

induced fuel swelling while Al cladding volume is preserved. Because the ATR-core side plate end has higher constraint by cladding, fuel volume transport occurs away from the fuel end and accumulates at a region, so-called bulge region toward the fuel width center (Fig. 2). Fission induced creep of U-Mo was conceived as the mechanism behind this phenomenon [2].

Although similar observations have been made for dispersion fuel plates, it is more difficult to quantify in this type fuel because of its complex microstructure that includes variations in fuel volume fraction in the meat, the presence of variable fractions of fuel-Al matrix interdiffusion products, and pore formed in matrix in some cases. Monolithic foil fuel plates do not have these obstacles, so this paper focuses on analyzing monolithic fuel plates, leaving the dispersion case for future work.

Finite element analysis (FEA) using a commercial code ABAQUS [3] was employed to examine whether the observed phenomenon is physically realistic by applying materials physical-mechanical parameters in reasonable ranges. Simultaneously, another objective of the FEA simulation was to obtain a creep rate coefficient that enables the extent of the fuel mass transport observed at the end of life (EOL) of the samples caused by creep.

2. Irradiation tests and post irradiation analyses

The samples used for this paper were from irradiation campaigns RERTR-6, -7, -8, -9A, -9B, -10, and -12. The sample fabrication and irradiation properties are summarized in Table 1. The plate dimensions are 100 mm in length, 25 mm in width, and 1.40 mm in thickness, which are a miniature version of full-size fuel plates used in research reactors and test reactors. The fuel foil dimensions are 82.6 mm in length and 19.0 mm in width. Foil thickness is typically 0.25 mm, and in some cases 0.50 mm is used.

The fuel foil is metallurgically bonded to Al 6061 cladding. Two kinds of bonding method were applied: One is friction stir welding (FSW) and the other hot isostatic pressing (HIP). As the name implies, the FSW method achieves a metallurgical bonding between the fuel foil and cladding by welding, in which cladding is instantaneously melted at the foil-cladding interface. The HIP method applies isostatic pressure of ~103 MPa while the plate is heated at 560 – 580 ^{o}C for 90 min. The details of the bonding methods can be found, for example, in Ref. [4]. It is worth noting that both bonding methods produce uniform bonding and, more importantly, do not alter foil thickness during the bonding processes.

The fuel plate samples were irradiated in the Advanced Test Reactor (ATR) at INL. The fission rate histories of samples are compared in Fig. 3. One representative sample from each test campaign is included.

The samples were loaded in the ATR in the manner that either a flat surface or a narrow edge faces the ATR core center. In the former case, called face-on loading, the power of the sample in the width direction is approximately symmetric and more uniform. Slight power peakings at the ends still exist due to the self-shielding effect. In the latter case, edge-on loading, the fission density of one edge of the sample that is closer to the ATR core is higher, as is illustrated in

Fig. 4. The power ratio of the high power edge to the low power edge is about 2.5 for HEU samples and about 2 for LEU samples (RERTR-6 plates), as determined in neutron physics analyses [5],[6].

After irradiation, the samples were sectioned at the axial mid-plane. The fuel cross section was metallographically examined as shown in
Fig. 4.

Table 1 Description of irradiation samples used in the analysis

Test	Plate ID	U-Mo foil property and plate fabrication method [a]	Enrichment (%U-235)	U-235 burnup, U-235-fissioned/U-235-initial (%)	Total duration (EFPD)	Fission density (10^{21} f/cm^3) [b]	BOL Fuel Temp (^{o}C) [c]
RERTR-6	L1F040	U-10Mo(f,n)	19.7	46	135	3.0	113
RERTR-7	L1F140	U-10Mo(f,n)	58.2	27	90	4.4	177
RERTR-9A	L1P04A	U-10Mo(p,n)	58.3	28	98	4.5	152
RERTR-9B	L1P05A	U-10Mo(p,n)	58.3	34	115	5.5	170
RERTR-12	L1P755 [d]	U-10Mo(p,n)	70.0	25	89	5.6	156

a: Number in front of Mo stands for Mo alloying content in weight%, b: Fuel volume average at EOL including fissions by Pu produced during irradiation, c: at fuel width center, d: face-on loading. All other samples were edge-on loaded to the center of the ATR (
Fig. 4), f: friction bonding, p: hot isostatic pressing bonding, n: as-fabricated foil thickness=0.25 mm, plate thickness = 1.4 mm, t: as-fabricated foil thickness=0.50 mm, plate thickness = 1.4 mm

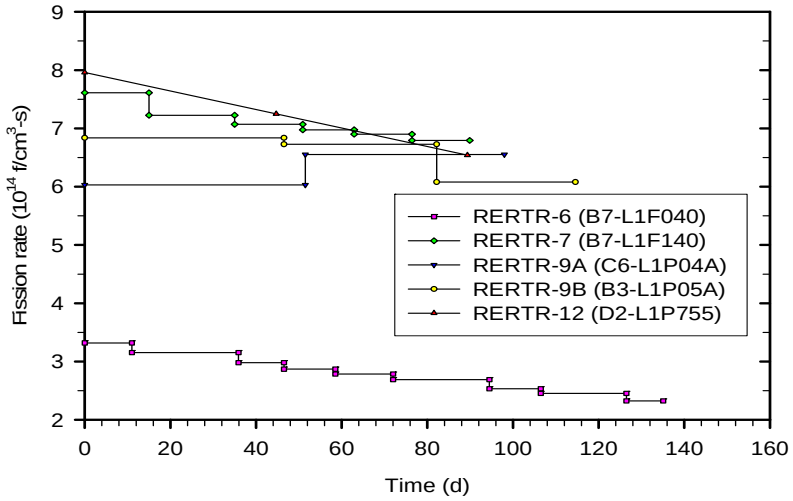

Fig. 3 Foil-averaged fission rate histories for representative samples.

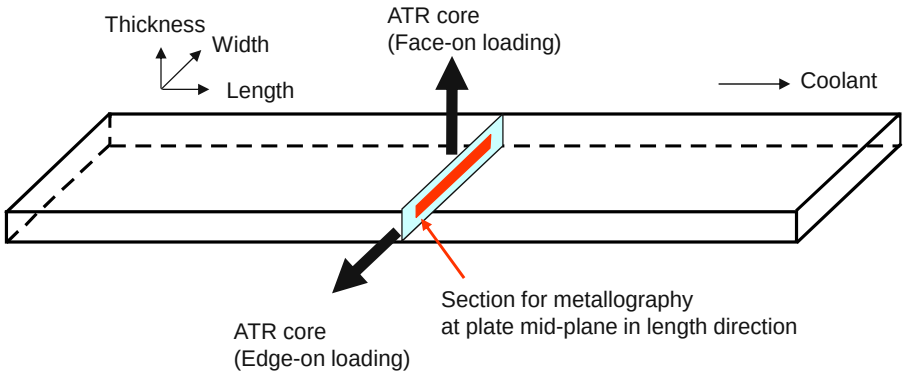

Fig. 4 Schematics of plate loading directions and PIE location

As said earlier, fuel swelling in a sample results only in plate thickness because the cladding is relatively unrestrained in the thickness direction. Therefore, once the post-irradiation foil thickness is known, fuel swelling can be quantified using the following equation:

$$\left(\frac{\Delta V}{V_0}\right)_f = \frac{\Delta t^f}{t_0^f} \qquad (1)$$

where Δt^f is foil thickness change after irradiation, and t_0^f is the as-fabricated foil thickness. Fuel swelling was also calculated by using the correlation available in the literature [1], and compared to measurement.

The measured fuel swelling data of L1P04A are plotted with the calculated in Fig. 5. The measured swelling at the tapered end of the foil, marked by A in Fig. 5, is substantially lower than the calculated value. In fact, it is even lower than the fuel swelling by solid fission products only. A and B, the areas enclosed by the measured fuel swelling curve and the calculated swelling curve, are the same magnitude. The similar observation is also made for C and D at the opposite end of the foil end. This salient phenomenon is commonly observed for all samples, although area comparisons are not perfectly consistent in some samples. The conclusion is that a mass transfer has occurred from A to B, facilitated by fission induced creep in the fuel as a response to an applied stress.

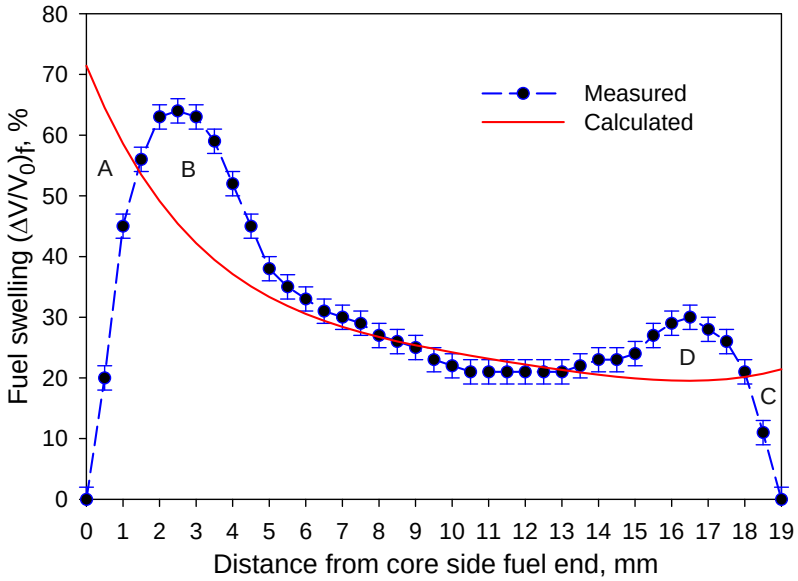

Fig. 5 Fuel swelling comparison between measured and calculated for L1P04A.

3. ABAQUS simulation

3.1. Input data

Young's modulus of 66 GPa and Poisson's ratio of 0.34 for Al6061 cladding are taken from Ref.[7]. Yield strength of the tempered Al alloys increases to ~280 MPa due to irradiation hardening [1]. This datum is used for Al6061 cladding considering fabrication and post-fabrication processes. Strain hardening of the Al-alloy cladding is taken into account. The strain hardening exponent of 0.13 for Al6061-T6 [9] is applied to cladding considering a decreased potential of strain hardening by neutron irradiation.

Young's modulus of U-Mo fuel of 85 GPa and Poisson's ratio of 0.34 are used for U-Mo alloy [7]. Yield strength of U-Mo is not needed in the simulation.

Fission-induced creep of U-Mo is dependent on the applied stress and fission rate. The following equation can be used to express the extent of U-Mo creep:

$$\dot{\varepsilon}_c = A\,\sigma\,\dot{f} \qquad (2)$$

where $\dot{\varepsilon}_c$ is the equivalent creep strain rate (s^{-1}), A the creep rate coefficient (cm^3/MPa), σ the equivalent stress (MPa), and $\dot{f}$ the fission rate (fissions/cm^3-s). Thermal creep is not considered because the temperature regime of interest is so low that this phenomenon is inactive.

The fuel swelling correlation from Ref. [1] is adopted:

$$\left(\frac{\Delta V}{V_0}\right)_f = 5.0\,f_d, \quad \text{for } f_d \le 3\times10^{21} \text{ fissions}/\text{cm}^3 \qquad (3)$$

$$\left(\frac{\Delta V}{V_0}\right)_f = 15 + 6.3(f_d - 3) + 0.33(f_d - 3)^2, \quad \text{for } 3\times10^{21} < f_d \text{ fissions/cm}^3 \qquad (4)$$

where fuel swelling is in percent and f_d is in 10^{21} f/cm^3. Note that the temperature effect is not considered in these equations.

Fuel true strain is obtained by converting fission product induced fuel swelling given in Eqs. (3) and (4) as follows:

$$\varepsilon_{f,true} = \ln\left[1 + \left(\frac{\Delta V}{V_0}\right)_f\right] \qquad (5)$$

3.2. Simulation for creep rate coefficient

The creep rate coefficient A in Eq. (2) is obtained by simulation of the U-Mo creep using ABAQUS FEA simulation.

The EOL condition of the plate L1P04A, which was irradiated with edge-on loading and has the same cladding thickness on both faces, was simulated. For this case, only an upper half of the fuel plate was modeled by symmetry. A schematic of fuel plate cross section and the FEA modeling scheme are shown in Fig. 6.

CPEG8R, generalized plane strain 8-node quadratic element with reduced integration, is used. A geometrically nonlinear analysis is applied to make more precise analysis based on the geometry

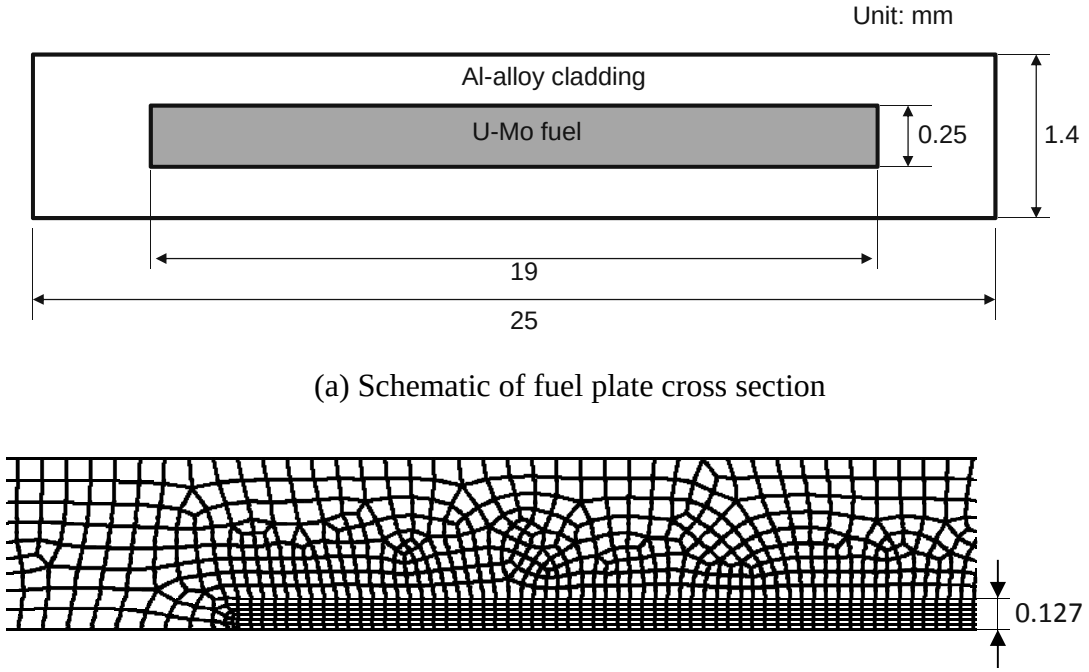

(a) Schematic of fuel plate cross section

(b) Finite element modeling

Fig. 6 Finite element modeling for L1P04A with edge-on loading and symmetric cladding thickness.

in the most recently completed increment. Again, bonding between fuel and cladding is assumed intact throughout life, which is inaccurate in some cases where debonding occurs.

FEA simulation was performed for fission product induced fuel swelling together with creep in L1P04A using several A values, and the best simulation was found when $A = 500 \times 10^{-25}$ cm^3/MPa, as shown in Fig. 7. The fuel swelling simulation plotted in Fig. 7(a) shows fair simulation of the swelling peaks at both fuel ends. As the creep coefficient increases, the peaks move toward the foil width center, and their apices become closer to the measured. However, fitting becomes worse again when A is increased greater than $A = 500 \times 10^{-25}$ cm^3/MPa.

The corresponding Von Mises stresses for the fuel swelling given in Fig. 7(a) are plotted in Fig. 7(b). It is considered that the stresses obtained with $A = 500 \times 10^{-25}$ cm^3/MPa is reasonable. The stress becomes zero at the foil end to satisfy the traction free boundary condition. It is also worth noting that the stress at the fuel central region in the width direction becomes smallest. The waviness nature in stress suggests that this uneven stress state may be the major driving force to cause separation of fuel foil from cladding during irradiation observed in some plates.

The simulation result of the combination of fission product induced fuel swelling and fuel mass transfer from the foil end to the foil central region in L1P04A is shown in Fig. 7(c). The FEA simulation also implies that fuel volume increase by fission product-induced fuel swelling at the foil end region is effectively removed and accumulated at the region showing peak foil thickness. Fuel flow is the highest at the foil thickness centerline and the lowest at the foil-cladding interface where the fuel is assumed to be perfectly bonded with the cladding.

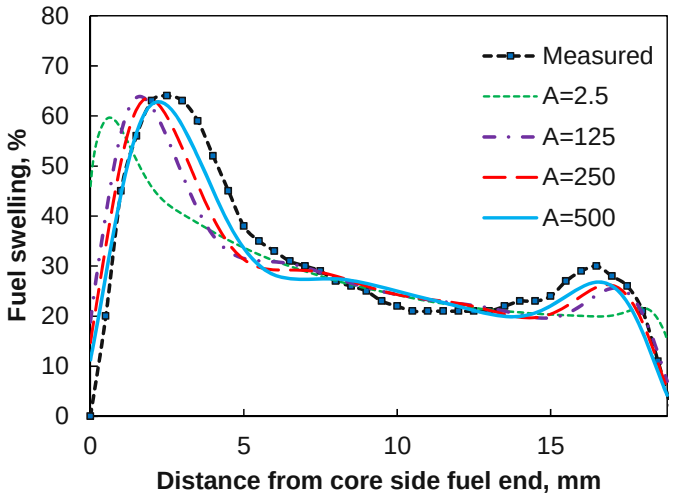

(a) Fitting fuel swelling for creep rate coefficient by comparing with the measured. A is in 10^{-25} cm^3/MPa.

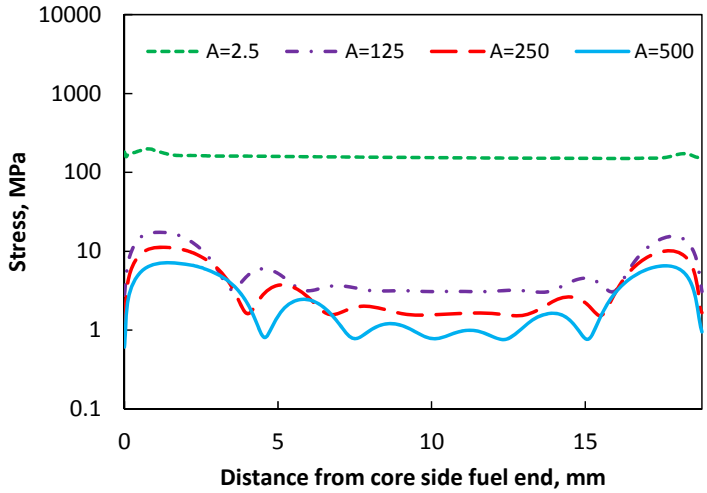

(b) Von Mises stress corresponding to the creep rate coefficient given in (a).

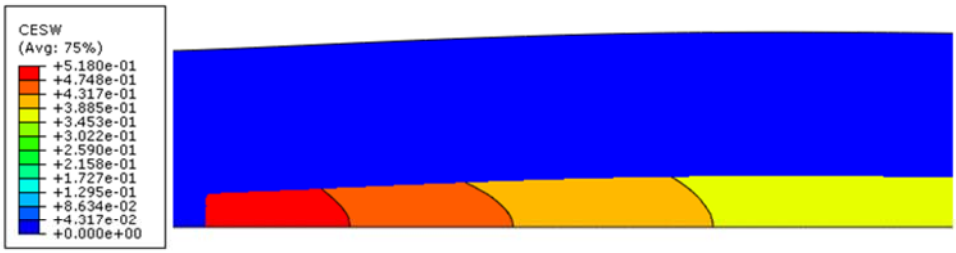

(c) Contour of fuel volume expansion by the combination of fuel swelling and creep-induced mass transfer from the foil end region to the foil central region

Fig. 7 Finite element simulation results to fit creep rate coefficient using the measured data for L1P04A.

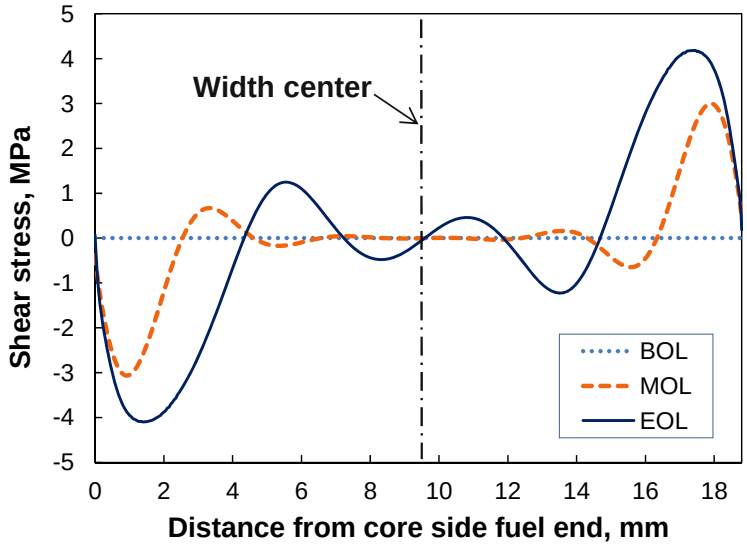

Fig. 8 Calculated shear stress at the foil-cladding interface at three points in irradiation time of L1P04A. Opposite sign across the center in the width direction is due to direction change.

The driving force for the mass transfer is provided by shear stress in the foil width direction. The evolution of the shear stress at the foil-cladding interface in the thickness direction is calculated at the beginning of life (BOL), middle of life (MOL) and end of life (EOL) and shown in Fig. 8. The shear stress increases as fission product induced fuel swelling increases and, as a result, mass transfer increases.

3.3. Validation of FEA simulation

The creep rate coefficient obtained in the previous subsection $A = 500 \times 10^{-25}$ cm^3/MPa and the FEA simulation results are examined by applying this value in simulation for other plates. Among the measured plates given in Error! Reference source not found., three plates with different fabrication geometry and plate loading direction are selected.

L1P04A is a plate having symmetric cladding thickness on both plate sides and edge-on loaded. L1P05A is a similar sample as L1P04A. FEA simulation was performed for L1P05A using the same creep rate coefficient, $A = 500 \times 10^{-25}$ cm^3/MPa. The FEA result is in reasonable agreement with the measurement (Fig. 9), although the simulated apex at the core side of L1P05A exhibits a slight discrepancy with the measurement.

L1P12Z was inadvertently fabricated with different cladding thickness on each side. FEA simulation was made for L1P12Z, using $A = 500 \times 10^{-25}$ cm^3/MPa, to include the effect of the asymmetric cladding thickness. The schematic of fuel cross section and the fuel FEA modeling scheme are shown in
Fig. **10**. The FEA results are shown in Fig. **11**. As shown in Fig. **11**(a), the FEA result is in excellent agreement with the measured for fuel swelling. Fuel deformation obtained by FEA

shown in Fig. **11**(b) occurs dominantly on the thin cladding side of the plate compared to the thick side, which is in accord with the metallography shown in Fig. **11**(c).

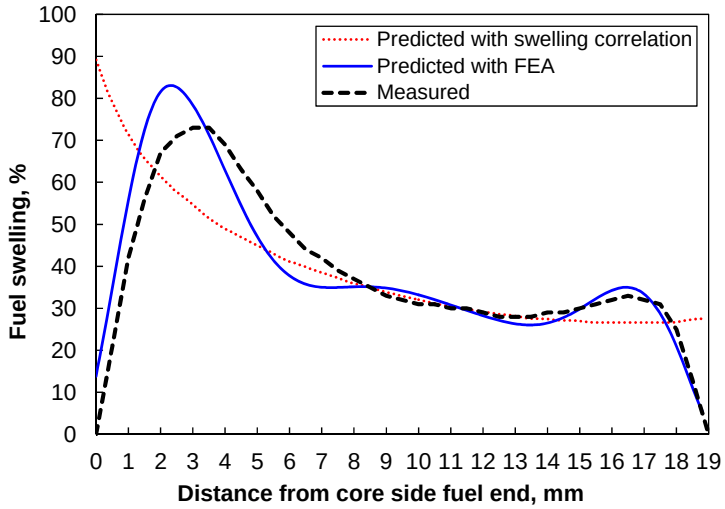

Fig. 9 Comparison of the predicted fuel swelling by FEA to the measured of L1P05A. The predicted fuel swelling by empirical correlation is also provided as reference.

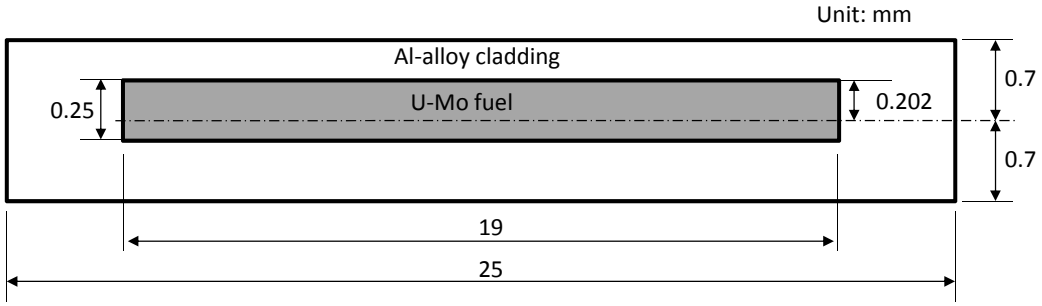

(a) Schematic of fuel plate cross section

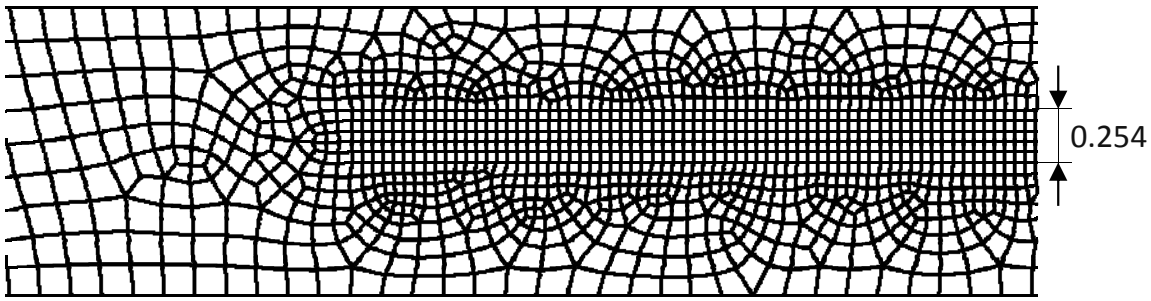

(b) Finite element modeling

Fig. 10 Finite element modeling for L1P12Z with edge-on loading and asymmetric cladding thickness on each side.

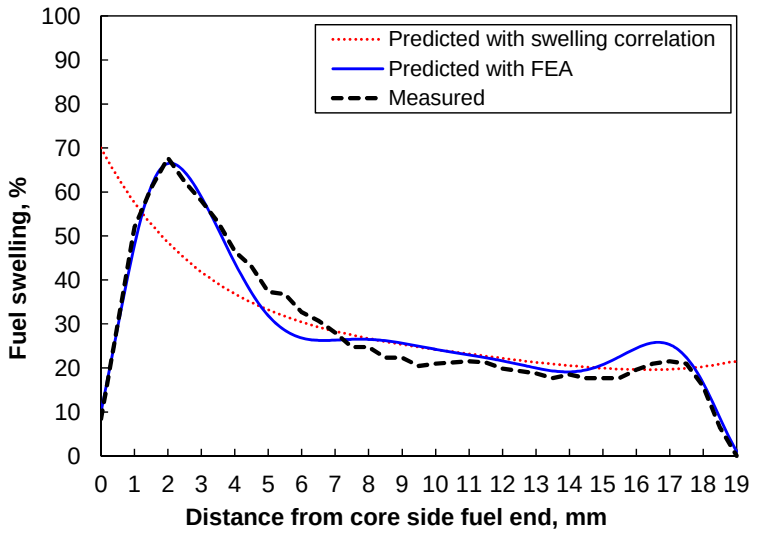

(a) Comparison of the predicted fuel swelling by FEA to the measured of L1P12Z. The predicted fuel swelling by empirical correlation is also provided as reference.

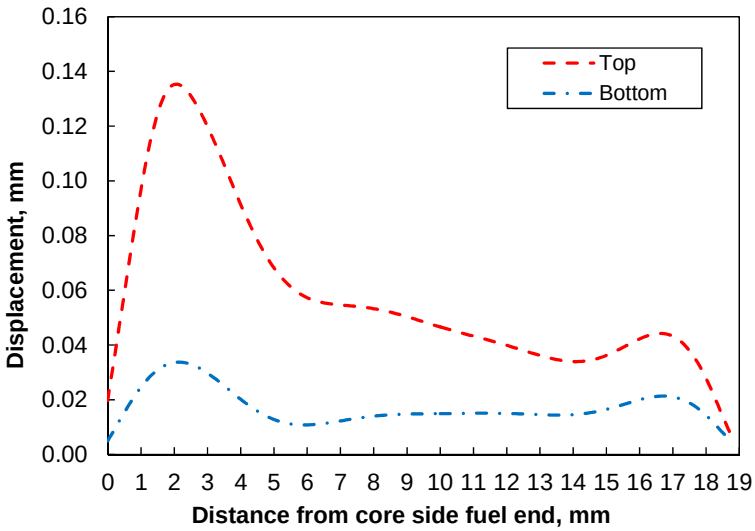

(b) Fuel displacements for both halves of the foil.

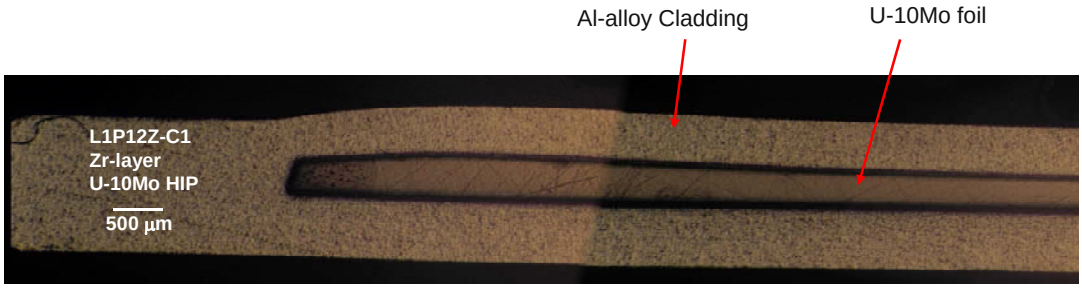

(c) Optical micrograph of cross section of L1P12Z in the width direction

Fig. 11 Finite element analysis results and PIE data of L1P12Z.

L1P755 from the RERTR-12 test is a face-on loaded. This loading scheme was employed to provide a more uniform power distribution across the plate width. However, gamma scanning during post-irradiation examination showed that power peaking still exists although less than the edge-on loaded plates as shown in Fig. 12(a). The FEA simulation result for L1P755, using $A = 500 \times 10^{-25}$ cm^3/MPa is shown Fig. 12(b) compares the FEA simulation result with the measured fuel swelling and the calculated fuel swelling without considering creep, in which the FEA simulation is consistent with the measured.

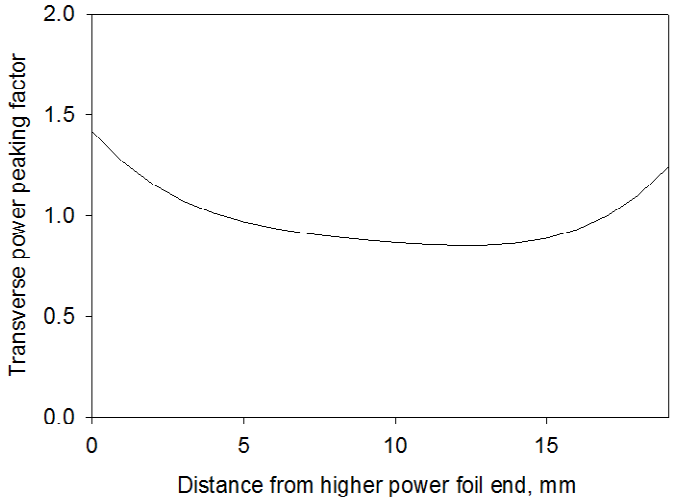

(a) Power peaking factors in the foil width direction measured by gamma scan

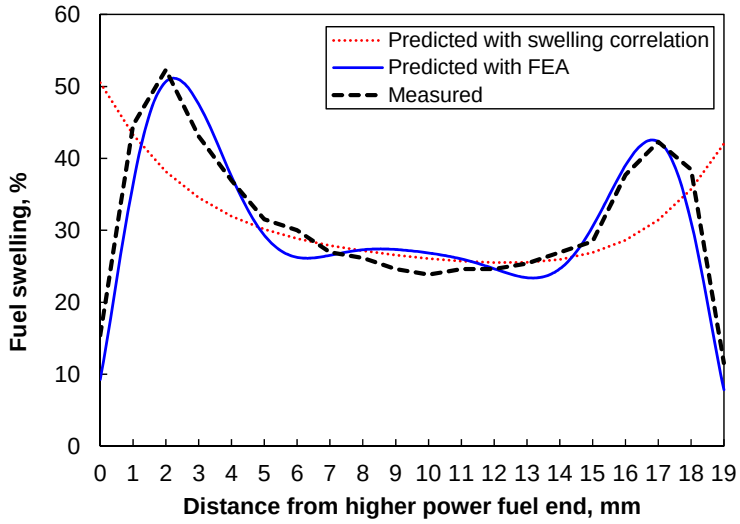

(b) Comparison of the calculated fuel swelling by FEA to the measured. The predicted fuel swelling by empirical correlation is also provided as reference.

Fig. 12 Power distribution across foil width and FEA analysis results for L1P755.

4. Discussion

The consistent FEA simulations with the measured data for L1P05A, L1P12Z and L1P755 using the creep rate coefficient $A = 500 \times 10^{-25}$ cm^3/MPa in general implies that the fuel mass transfer is indeed enabled by a creep mechanism and that ABAQUS FEA is applicable in simulation of the fission induced creep observed for U-Mo alloy fuel regardless of fuel fabrication and loading types. ABAQUS FEA also demonstrates that not only the obtained creep rate constant is acceptable, but also the FEA modeling itself is valid in simulating the measured data.

Fission enhanced creep at low homologous temperatures was observed in all nuclear fuels and was first identified in α-U in the 1950s by Russian [10]and British [11] workers, and subsequently in ceramic fuels by various researchers [12]-[18]. Common for all, the creep rate was found to be athermal, and have a linear dependence on the applied stress and fission rate, as is the case in Eq. (2). The obtained creep rate coefficient $A = 500 \times 10^{-25}$ cm^3/MPa is compared with other U-fuels in the literature at homologous temperatures relative to their melting points in Table 2. The obtained value lies between pure uranium and MOX. It turns out that the value for U-10Mo is rather high, higher than ceramic fuels, and reaching nearly that of pure uranium (orthorhombic), which means the alloying of 10wt% Mo does not significantly reduce the creep rate. The reason for this may be because during irradiation, U-10Mo is in the γ-phase without formation of any precipitate phases [1],[20],[21] that affects the creep rate, and the slightly lower creep rate in the γ-phase (bcc) U-10Mo is most likely due to the phase change from a denser phase α-phase (orthorhombic).

Table 2 Creep rate coefficient (A) in Eq. (2)

Fuel	A (10^{-25} cm^3/MPa)	~T/T_m	Reference
U	800	0.3	[10], [13]
U-10wt.%Mo	500	0.3	Present study
MOX	56	0.25	[14]
UO_2	7	0.25	[15],[16],[17]
UN	3	0.3	[18], [18]
UC	1	0.3	[17]

The high creep rate enables the extent of observed fuel lateral mass transfer, which is the effective mechanism that lessens the stresses at the foil end region caused by fission product induced fuel swelling where peak fission density is usually achieved. This mechanism allows U-Mo fuel to achieve high burnup without failure, by reducing the potential to plate buckling. The high creep rate can also explain the extent of fuel particle deformation observed in high burnup dispersion fuel plates shown in Fig. 13, in which the spherical U-Mo particles, when they were as-fabricated, underwent significant deformation during irradiation. This sample also shows sintering between particles. The analysis of creep behavior of the dispersion fuel samples is not pursued in this work.

The rather large increase in local fuel loading at the peak thickness location resulting from the lateral fuel creep may have to be considered for hot-spot calculations for reactors that operate fuel at high power after substantial burnup by the use of burnable poisons. The additional plate thickness increase by creep in addition to fission product induced fuel swelling at the peak thickness location must be incorporated in safety analyses. The additional foil thickness increase by creep is ~25% from the as-fabricated foil thickness at a fission density of $7x10^{21}$ f/cm^3, which is considerable in a safety analysis.

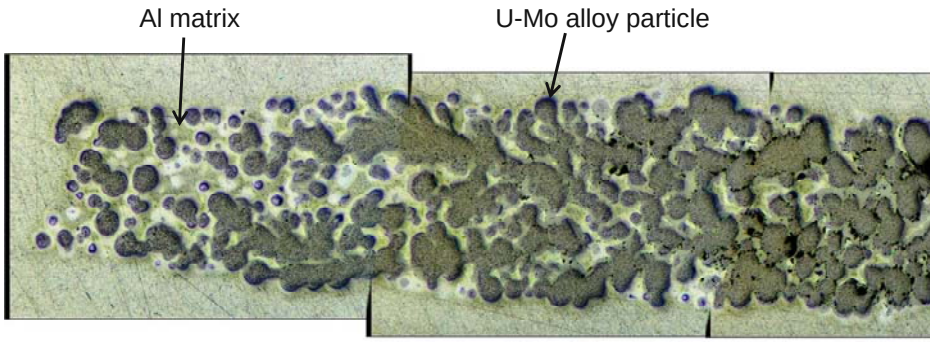

Fig. 13 Optical micrograph of fuel meat end region of R6R018 where the meat-averaged fission density is ~$10x10^{21}$ f/cm^3-fuel-particle.

An implication from this work that affects the measurement of fission product induced fuel swelling is that one must avoid measuring it at or near the foil end regions. Measurements at these regions will lead to erroneous results affected by fuel lateral mass transfer.

5. Conclusions

The tapered U-Mo fuel foil observed at the foil width end region, where fission density is highest, has been reviewed. The underlying mechanism is lateral mass transfer by fission induced creep, which is athermal and dependent on stress that builds up by fission product induced fuel swelling and fission rate in the area. The creep of U-Mo fuel is the effective mechanism that lowers the stresses at the foil end region where fission product induced fuel swelling is the highest because of peak fission density there, and enables U-Mo alloy fuel to achieve high burnup without failure.

ABAQUS finite element analysis (FEA) simulation coupled with the model for fission product induced fuel swelling and creep model produced consistent results with the measured fuel swelling data for all fuel plate types and loading schemes with physical-mechanical data available in the literature. This proves that the fuel mass transfer is indeed by creep mechanism and validates that ABAQUS FEA is applicable in simulation of the fission induced creep observed for U-Mo alloy fuel.

ABAQUS simulation also produced the best-fit creep rate constant for U-10Mo alloy fuel $500x10^{-25}$ cm^3/MPa, which lies between pure uranium and MOX, and greater than other ceramic uranium fuels.

Acknowledgments
The authors would like to thank Mrs. C. Clark, G. Moore, and J. Jue for the fabrication of the samples used in this work. The operations staff at ATR is also acknowledged for the irradiation tests. The physics data available by Dr. G. Chang and Ms. M. Lillo are also appreciated. This work was supported by the U.S. Department of Energy, Office of Global Threat Reduction (NA-21), National Nuclear Security Administration, under Contract No. DE-AC-02-06CH11357 between UChicago Argonne, LLC and the Department of Energy.

References

[1] Y.S. Kim, G.L. Hofman, J. Nucl. Mater., 419 (2011) 291.
[2] G.L. Hofman, Y.S. Kim, A.B. Robinson, Trans. 13th Internat. Topical Meeting Research Reactor Fuel Management (RRFM), RRFM 2009, Vienna, Austria, March 22 -25, 2009. http://www.euronuclear.org/meetings/rrfm2009/index.htm
[3] ABAQUS Analysis User's Manual, Dassault Systems, 2011.
[4] C.R. Clark, J.M. Wight, G.C. Knighton, G.A. Moore, J.F. Jue, the 27th International Meeting on Reduced Enrichment for Research and Test Reactors (RERTR), Boston, Massachusetts, November 6-10, 2005. http://www.rertr.anl.gov/RERTR27
[5] M. A. Lillo, "MCNP-calculated gradients across RERTR-6 and RERTR-7 miniplates irradiated in ATR," Interoffice Memo, INL, 2007.
[6] G. S. Chang, M. A. Lillo, 2008, "As-Run Neutronics Analysis of the RERTR-9A/B Capsules in the ATR B 11 Position," Engineering Calculations and Analysis Report -231, 2008.
[7] J.S. Cheon, Y.S. Kim, Material Properties of Aluminum Alloys and Pure Zirconium for Use in High-density Fuel Development for Research Reactors, ANL/RERTR/TM-12-6, 2012.
[8] A.M. Nomine, D. Bedere, D. Miannay, Proc. Coloque sur la rupture des materiaux, Grenoble, 9-21 January 1972.
[9] Y. Tamarin, Atlas of Stress-Strain Curves, Materials Park, Ohio, ASM International, 2002.
[10] S.T. Konobeevsky, N.E. Pravdyuk, V.I. Kutaitsev, UN Int'l Conf. Peaceful Use of Atomic Energy, Geneva, Switzerland, Paper no. 681, 1955.
[11] A.C. Roberts, A.H. Cottrell, Phil. Mag., 1 (1956) 711.
[12] A.S. Zaimovsky, UN Int'l Conf. Peaceful Use of Atomic Energy, 1958.
[13] M. Hesketh, Discussion in paper: M. Englander, C. T. Montpreville, 11th Colloque de Metallurgie, Creep, June 1967, p.28, Centre D'Etudes Nucleaires de Saclay, 1968.
[14] R. J. White, The Re-irradiation of MIMAS-MOX Fuel in IFA-629.1, HWR-586, March, 1999.
[15] A.A. Solomon, J. Am. Ceram. Soc., 56 (1973) 164.
[16] W. Dienst, J. Nucl. Mater., 65 (1977) 1.
[17] D.J. Clough, J. Nucl. Mater., 65 (1977) 24.
[18] D. Brucklacher, W. Dienst, Proc. Am. Ceram. Soc., Anaheim, California, USA, Nov. 1971.
[19] P. Zeisser, G. Maraniello, P. Combette, J. Nucl. Mater., 65 (1977) 48.
[20] M.L. Bleiberg et al., J. Appl. Phys., 27(11) (1956) 1270.
[21] M.L. Bleiberg, J. Nucl. Mater., 2 (1959) 182.